ELSEVIER

Nuclear Instruments and Methods in Physics Research A 433 (1999) 104–120

NUCLEAR INSTRUMENTS & METHODS IN PHYSICS RESEARCH Section A

www.elsevier.nl/locate/nima

The AQUA-RICH atmospheric neutrino experiment

P. Antonioli[a], G. Bari[a], L. Bellagamba[a], E. Chesi[b], F. Cindolo[a], S. De Pasquale[a], T. Ekelof[c], M. Garbini[a], P. Giusti[a], A. Grossheim[h], A. Pesci[a], J. Learned[d], A. Margotti[a], J. Pinfold[e], G. Sartorelli[a,f], J. Seguinot[g], A. Tarantino[a,f], P. Weilhammer[b], Th. Ypsilantis[a,*], A. Zichichi[a,f], K. Zuber[h]

[a]*University of Bologna, INFN Bologna, Via Irnerio, 46, 40126 Bologna, Italy*
[b]*University of Bologna, CERN, Geneva, Switzerland*
[c]*University of Uppsala, Uppsala Sweden*
[d]*University of Hawaii, USA*
[e]*University of Alberta, Canada*
[f]*University of Bologna, Bologona, Italy*
[g]*College de France, Paris, France*
[h]*University of Dortmund, Dortmund Germany*

Abstract

We describe a 125 m diameter spherical detector containing 1 Mt of water, capable of high rate observation of atmospheric neutrino events (30 000/y). The ring imaging Cherenkov (RICH) technique is used to measure velocity, momentum and direction of particles produced by neutrinos interacting in water. The detector will be sited outdoors (under a 50 m water shield) in a natural (further excavated) pit, probably in Sicily.

Spherical reflecting mirrors focus Cherenkov light produced by secondaries from interacting neutrinos. Photons are detected by 5310 hybrid photodiodes (HPDs) of 1 m diameter each with 396 pads of 45×45 mm^2 on the photocathode surface, demagnified to 9×9 mm^2 on the silicon sensor. For most tracks the ring width will be dominated by multiple scattering which should allow momentum to be determined. Hadrons of momentum $p \leq 5$ GeV/c can be measured with $\sigma_p/p \leq 7\%$ and muons of $p \leq 32$ GeV/c with $\sigma_p/p \leq 1\%$. The ring center determines track direction with $\sigma_{\theta x}$, $\sigma_{\theta y} \approx 6$ mrad. Track reconstruction in water will require time resolution $\sigma_t < 1$ ns.

Detection of oscillating muon signals (disappearance) is feasible with atmospheric neutrinos and precision measurement of oscillation parameters is feasible for $10^{-2} \leq \Delta m^2 \leq 10^{-4}$eV^2. Tau or sterile neutrino appearance experiments are also possible with atmospheric neutrinos. Other physics topics addressable with this detector are proton decay, supernova detection and search for astrophysical neutrino sources.

A first test module of 3 tons water and 120 PMs (32 mm ϕ) will operate (5/99) with 1–3 GeV muons in a CERN-PS test beam to verify the momentum algorithm. A second (6 m)^3 test module with 216 tons of water and 25 HPDs (0.25 m ϕ) is designed to observe full multi-track images and test pattern recognition and ring reconstruction algorithms.

1. The AQUA-RICH experiment

The large water volume of AQUA-RICH is intended to detect and measure interactions of

* Corresponding author.
E-mail address: at.ypsilantis@cern.ch (Th. Ypsilantis)

0168-9002/99/$ - see front matter
PII: S0168-9002(99)00542-2

atmospheric or long baseline beam neutrinos. Cherenkov photons produced by charged secondaries arising from the neutrino interaction are focused by spherical mirrors and detected by fast, position-sensitive Hybrid Photo Diodes (HPDs). The experiment was submitted to the Gran Sasso laboratory (1/1/96) on the occasion of their call for long baseline proposals [1]. Later papers, now available, describe the experiment in more detail and give some analysis techniques for pattern recognition and reconstruction of ring images [2,3].

Water is, of course, cheap and safe and serves both as the neutrino target and the radiating medium. Cherenkov photons produced by charged particles from neutrino interactions in the water are detected with visible light photo-sensors. The essential hardware elements of this experiment, i.e clean water, photomultipliers (PMs) and mirrors are completely proven and do not require additional R&D. The first two of these elements were used in the pioneering IMB and Kamiokande experiments and are present in the operating 50 kt Super-Kamiokande detector which investigates solar and atmospheric neutrino interactions as well as proton decay.

Our technique differs in one essential aspect namely, the use of a mirror to give focused images which allows particle velocity to be determined from ring radius and direction from ring center. In addition, particle momentum can be determined from ring width if multiple scattering is the dominant aberration. Without a mirror, the ring width is dominated by particle track length which prohibits measurement of multiple scattering. Clearly, if velocity and momentum are known then mass is determined. Track length is of course interesting for physics but it can be otherwise determined from the number of photons in the ring. Moreover, particle charge (but not its sign) is found by measuring the density of hit points on the ring circumference.

Formation of focused rings obviously facilitates pattern recognition. Without mirror, a normally directed track of length L at distance D from a photosensor plane makes a ring of width $\Delta w = L \tan\theta$ and radius $r = D \tan\theta$ hence $\Delta w/r = D/L$. For example, a 2 GeV/c muon in water ($\theta \approx 0.73$) has $L \approx 10$ m and $D = 20$ m (the average value in Super-K) hence $\Delta w/r = 0.5$ i.e the ring is half filled. With a mirror of focal length f, the ring radius $r = f\theta$ and width $\Delta w \approx 2.35 f\sigma_\theta$ but in AQUA-RICH $\sigma_\theta \leq 10$ mrad thus $\Delta w/r \leq 2.35\sigma_\theta/\theta = 0.032$. Consequently, for ring widths which are only 3% of the radius, we can recognize and reconstruct multiple rings ($n \leq 4$) whereas in Super-K, with ring widths $\geq 50\%$ of their radius, multiple rings overlap and are much more difficult to recognize.

A unique feature of AQUA-RICH lies in its ability to measure the total energy of the quasi-elastic ($\nu_\mu n- > \mu^- p$) or resonance elastic ($\nu_\mu n- > \mu^- \Delta^{++}$) events hence muon disappearence will manifest itself as a hole in the wideband ν_μ energy spectrum.

For produced electrons and gammas AQUA-RICH represents a homogeneous Cherenkov calorimeter (water being the showering and radiating medium) with energy resolution $\sigma_{Ee}/E_e \approx 12\%/\sqrt{E_e(\mathrm{GeV})}$ for detector response $N \approx 1500$ pe/GeV.

2. The AQUA-RICH detector

2.1. Site

Placement of AQUA-RICH inside a hall of Laboratorio Nazionale Gran Sasso (LNGS) has several major disadvantages:

(i) its unit cost is much higher than for outside placement;
(ii) it would fully occupy Hall B or C, both attributed to other experiments;
(iii) its mass would be limited to 17 kt in Hall B or 29 kt in Hall C;

Therefore, we consider large outside detectors capable of high rate observation of both atmospheric and long baseline beam events. The best site at LNGS for the detector would be at the end of Campo Imperatore or on the downstream slope of Mt. Bolza where the neutrino beam exits earth and the neutrino flux is maximum but this area is part of a protected park where building or excavation is prohibited.

For this and other reasons (better sensitivity) we prefer a purely atmospheric experiment located in a convenient non-mountainous area where

building is easier and cheaper. Moreover, the distance from CERN should be maximum (but still in Europe to allow for possible future long baseline beams) and have a good climate for ease of construction. Indeed, we are investigating a natural ravine in Sicily where AQUA-RICH could be sited.

2.2. Geometry

Spherical geometry is well adapted to detect omni-directional neutrinos with high efficiency. The detector would be built in a 125 m diameter, 175 m deep pit with base and concrete walls lined with plastic sheets and filled with water. The upper 50 m of water acts as a shield to stop downward muons $\leq 10\,\mathrm{GeV}/c$ thus reducing detector occupancy. Besides neutrino oscillations, other physics topics which can be investigated in such a large detector are proton decay, neutrinos from supersymmetric particles or astrophysical sources i.e AGNs, GRBs, Blazars and SuperNovae (3ν events/burst at distance of 1 Mpc).

The schematic view of Fig. 1 shows two spherical domes in a water-filled cylindrical hole, 125 mϕ and 175 m deep. The 125 m $\varnothing$ outer surface is defined by an inflated balloon which is both reflective and spherical. This is achieved by "cutting to size" a mylar–Al–mylar fiber and welding together segments tailored to give a spherical shape when inflated. The concentric 62.5 m ϕ inner dome is 20% covered by 3125 outward facing 1 m ϕ detector (d)HPDs, i.e one dHPD per $2\times 2\,\mathrm{m}^2$ grid. The geodesic domes are constructed with kevlar (or stainless steel) struts linking nodes. In addition, 2185 inward facing mirror (m)HPDs uniformly cover 3.5% of the outer dome (through un-aluminized areas left on the mirror surface) hence a total of 5310 HPDs. For atmospheric neutrinos only the upward and downward $4\pi/3$ sterad (i.e $\leq 70^\circ$ to the zenith) are useful to detect the oscillation pattern (see Section 3.2) hence only 2/3 of the surfaces need be instrumented (i.e 3540 HPDs of 1 m ϕ with 1.4 Mpixels). For comparison, Super-K has 11200 PMs of 0.5 m ϕ with 11.2 kpixels.

A photon not detected in its first pass through the outer dome will be easily recognized because, if detected in its second pass, it will be delayed by ≥ 558 ns (a similar argument holds for mHPD hits). For a photo-absorption length achievable in water $l_w \approx 100$ m and 10% loss at each mirror reflection (5% due to mirror reflectivity and 5% due to mHPDs and dead areas) and 20% loss at each traversal of the dHPD surface, the effective absorption length $l_{\mathrm{abs}} \approx 69$ m hence 16% of the photons will survive one pass but only 2.7% the second pass.

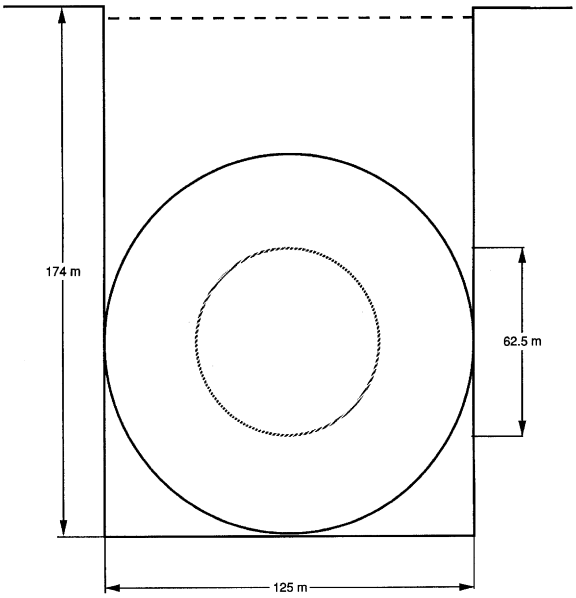

Fig. 1. A schematic view of the 1 Mt AQUA-RICH experiment. The 125 m diameter reflective balloon is made of an mylar-aluminum-mylar sandwich inflated by a small N_2 gas pressure ($=100$ mbar). The 125 m diameter outer geodesic dome supports 2185 inward looking mHPDs which cover 3.5% of the dome surface and collect Cherenkov photons through un-aluminized areas in the mylar balloon. The 62.5 m diameter inner geodesic dome supports 3125 outward looking dHPDs which cover 20% of the dome. The dotted line shows the water level. Not shown are two ground level crane installations and a corrugated industrial roof covering the pit.

The balloon center is oriented to coincide with the dome centers at $z = x = y = 0$. For the average image distance $\langle q\rangle \approx 31.25$ m the ring diameter ($d_{\mathrm{im}} \approx 2\langle q\rangle\theta$) of 46 m is well contained on the 62.5 m ϕ detector dome.

2.3. The HPD photo-sensors

The HPD is made in a 1016 mm diameter (40″) glass envelope with a 1000 mm diameter bialkali

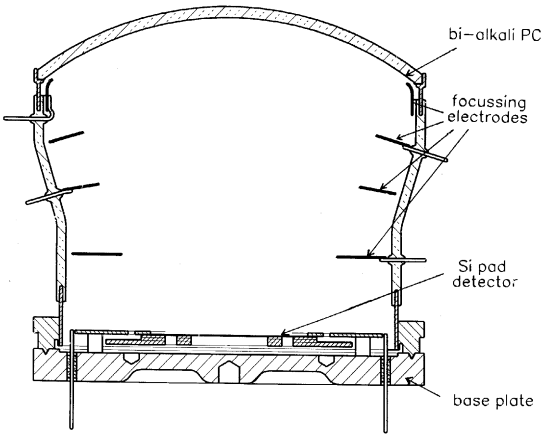

Fig. 2. A schematic view of an HPD with tube diameter and length each 1 m. The vacuum photocathode is deposited on the inner window surface. The electrodes focus the produced photoelectrons onto a 200 mm diameter (4 wafer) silicon sensor with 396 hexagonal pixels. A trace from each pixel is brought to the sensor circumference and wire bonded to one input of the 4-128 channel readout chips.

vacuum photocathode (PC) and four focusing electrodes, similar to the 254 diameter (10″) HPD built for the AQUA-RICH test modules (see Fig. 2).

The photon energy acceptance of the dHPDs will be limited to 0.6 eV (by a thin absorbing film on the glass entrance window) in order to reduce chromatic aberrations and so to maximize sensitivity for measuring multiple scattering. For 20% dHPD cover about $460L\varepsilon_g\varepsilon_a$ photon hits will be detected from a track with pathlength L(in meters). Here ε_g is geometrical efficiency for photon imaging (obtained from simulation for specified track parameters) and ε_a is the photon transmittance in water. Because the mHPDs are only used to measure the track parameters (the vertex 4 vector and track direction), multiple scattering sensitivity is not required so the photon energy acceptance can be increased to ≈ 1.7 eV hence, for the 3.5% mHPD cover, about $230L\varepsilon_g\varepsilon_a$ mHPD hits will be detected.

Each HPD has 396 hexagonal pads of 9×9 mm^2 on the 200 mm ϕ silicon sensor corresponding to 45×45 mm^2 on the PC surface (i.e electrostatic demagnification by factor 5 in the HPD). Four 128 channel readout chips are installed in the HPD vacuum envelope. A signal trace from each HPD pad is brought to the silicon sensor periphery where it is wire bonded to one channel of a readout chip. Each channel has a front-end amplifier, an 80 MHz analogue sampling pipeline, control logic, command decoder and output multiplexer. Since the HPD single-electron response function has very little amplitude variation, it suffices to readout 16 samples of the pulse waveform to accurately determine the pulse time with $\sigma_t < 1$ ns. Each pad signal has a different fixed time delay (pre-determined and therefore correctable) however, the variance of the photoelectron arrival time is only 50 ps thus, given the expected noise level and precision of the waveform digitization, a highly precise ($\sigma_t \approx 100$–200 ps) time measurement is expected. A coincidence of ≥ 100 dHPD pad hits in a ≈ 50 ns time window preceeded by ≥ 50 mHPD pad hits ≈ 140 ns earlier will signal an interesting event and start readout.

To attain the best precision on track velocity and momentum from the hit pattern on the detector plane, we must reconstruct the Cherenkov angles in the particle reference frame [3]. This requires determination of the track parameters, i.e the particle direction (θ_p, ϕ_p), the interaction vertex point ($\boldsymbol{r}_v$,t_v) and the photon emission point ($\boldsymbol{r}_e$, t_e). These parameters are strongly constrained by the measured hit points ($\boldsymbol{r}$, t) in the dHPDs and ($\boldsymbol{r}_m$, t_m) in mHPDs (see Section 5).

2.4. Photoelectron hits and Cherenkov angle resolution

The number of dHPD hits per unit track pathlength for PC cover $f_{pc} = 0.2$, energy acceptance $\Delta E = 0.6$ eV (i.e 2.3–2.9 eV), mirror reflectivity $R = 0.95$ and quantum efficiency $Q = 0.25$ is $N/L = (37/\text{eV-mm}) \times \sin^2\theta \times Q \times R \times \Delta E x f_{pc} = 467/\text{m}$ hence the detector merit factor $N_0 = N/L \sin^2\theta = 1060\ \text{m}^{-1}$.

The Cherenkov angle θ is given by Cherenkov's equation $\cos\theta = 1/n\beta$ where $n(E)$ is the water refractive index, E is the photon energy and β the particle velocity ($\theta = 727$ mrad for $\langle E \rangle = 2.6$ eV and $\beta = 1$). The Cherenkov angle error due to pad size $\sigma_\theta(xy) \approx \sigma_x/q = 0.42$ mrad is chosen small (i.e $\sigma_x = \Delta x/\sqrt{12}$, $\Delta x = 45$ mm and $q = 31.25$ m) compared to the chromatic dispersion $\sigma_\theta(E) \approx 1.5$ mrad so that their quadratic sum $\sigma_{\theta 0} \approx 1.56$ mrad is

about equal to the multiple scattering width $\sigma_\theta(ms) \approx 1.7$ mrad for a 5 GeV/c track of length $L = l_{abs} = 85$ cm.

2.5. Momentum measurement in AQUA-RICH

When multiple scattering aberrations dominate the ring width then momentum can be obtained from the relation

$$\sigma_\theta = \sigma_\theta(ms) = \frac{k_{ms}}{p\beta}\sqrt{\frac{L}{X_0}} = \frac{k_{ms}}{m\gamma\beta^2}\sqrt{\frac{L}{X_0}} \quad (1)$$

where the radiation length of water $X_0 = 36$ cm and $k_{ms} = 13.6/\sqrt{6} = 5.55$ MeV. The latter is reduced by $\sqrt{6}$ from the standard value of 13.6 MeV because of the shorter average pathlength before radiating ($\frac{1}{2}$) and correlations in the multiple scattering angle ($\frac{1}{3}$). Inserting the θ dependance of $\beta(=1/n\cos\theta)$ and the (θ,N) dependance of $L(=N/N_0\sin^2\theta)$ gives

$$p = \left(\frac{K}{\tan\theta}\right)\sqrt{\frac{N}{(\sigma^{2\theta} - \sigma^2_{\theta_0})\varepsilon_g\varepsilon_a}} \quad (2)$$

where $K \equiv nk_{ms}/\sqrt{(N_0X_0)}$ and $\sigma_{\theta 0}$ is the ring width from all non-momentum dependent sources. Recalling that $N_0 = 1060\ \mathrm{m}^{-1}$ and for water ($n = 1.34$) then $K = 0.38$ MeV. The mass equation $m = p/\beta\gamma$ in terms of the same variables (θ,σ_θ,N) becomes

$$m = \left(\frac{nK}{\tan\theta}\right)\sqrt{\left(\frac{\sin^2\theta_m - \sin^2\theta}{\sigma^2_\theta - \sigma^2_{\theta_0}}\right)\frac{N}{\varepsilon_g\varepsilon_a}} \quad (3)$$

where $\cos\theta_m = 1/n$. From Eqs. (2) and (3) we obtain for the momentum and mass errors

$$\frac{\sigma_p}{p} = \sqrt{\frac{(1/4) + (\varepsilon^2/2) + (\tan\theta\sigma_\theta/\sin^2\theta)^2}{N}} \quad (4)$$

$$\frac{\sigma_m}{m} = \sqrt{\frac{(1/4) + (\varepsilon^2/2) + [(\gamma^2 + 1/\sin^2\theta)\tan\theta\sigma_\theta]^2}{N}} \quad (5)$$

where $\varepsilon \equiv \sigma^2_\theta/(\sigma^2_\theta - \sigma^2_{\theta 0})$ i.e $\sigma_\theta = [\varepsilon/(\varepsilon - 1)]^{1/2}\sigma_{\theta 0}$. For multiple scattering dominance (MSD) then $\varepsilon \approx 1$ and the first two terms in the numerator of Eq. (4) are $\frac{3}{4}$ while the third term is negligible hence $\sigma_p/p \approx 0.87/\sqrt{N}$. For $L = l_{abs} = 850$ mm then N ≈ 391 and $\sigma_p/p \approx 4.4\%$ showing that, in principal, good momentum resolution is possible.

A 5 GeV/c hadron track with average pathlength $L = 0.85$ m has multiple scattering width $\sigma_\theta(ms) \approx 1.7$ mrad, chromatic width $\sigma_\theta(E) \approx 1.5$ mrad and pad width $\sigma_\theta(xy) \approx 0.42$ mrad hence $\sigma_{\theta 0} \approx 1.55$ mrad, $\varepsilon = 1.83$ and $\sigma_p/p \approx 7\%$. Thus, for an average pathlength hadron track, MSD extends to 5 GeV/c but most hadrons produced by 1–20 GeV ν interactions have $p \ll 5$ GeV/c thus the problem of measuring higher momenta concerns only muons (e-showers are fully contained in $20X_0 = 7.2$ m).

For 1 Mt AQUA-RICH in the spherical geometry of Fig. 1, an average high energy muon has pathlength $L \approx 62.5$ m, $N \approx 29375$ and $\sigma_\theta(ms) \approx$ (73 mrad GeV)/p thus MSD ($\varepsilon \leq 2$) applies for $p_\mu \leq 32$ GeV with resolution $\sigma_p/p = 0.9\%$. Of course, this will only be possible if the emission point error $\sigma_\theta(u_e)$ can be suppressed via the good-time measurements.

3. Atmospheric neutrinos

3.1. Fluxes and rates

The atmospheric ν_μ (and $\bar{\nu}_\mu$) fluxes are adequately approximated by the simple analytical expression

$$\frac{d\phi_{\nu_\mu}}{dE_\nu} = \frac{d\phi_{\bar{\nu}_\mu}}{dE_\nu} = \frac{\phi_0}{E^3_\nu} \quad (6)$$

where $\phi_0 \approx 0.025\ \mathrm{GeV}^2/\mathrm{cm}^2$-ster-s is the average over the zenith angles $0^0 < \Theta < 70^0$ and energies $1 < E_\nu < 20$ GeV [4,5]. The neutrino-nucleon cross section increases with neutrino energy as $\sigma = \sigma_0 E_\nu$ with $\sigma_0 = 0.67 \times 10^{-38}\ \mathrm{cm}^2/\mathrm{GeV}$, $\sigma_{0\nu_\mu} = \sigma_0$ and $\sigma_{0\bar{\nu}_\mu} = 0.5\sigma_0$ thus the muon event rate is

$$\frac{d^2N}{d\Omega\, dt} = n_0(\phi_{\nu_\mu}\sigma_{\nu_\mu} + \phi_{\bar{\nu}_\mu}\sigma_{\bar{\nu}_\mu}) = n_0\phi_0\sigma_0 \times \int\left(\frac{E_\nu dE_\nu}{E^3_\nu} + \frac{1}{2}\frac{E_\nu\, dE_\nu}{E^3_\nu}\right) = \frac{3}{2}n_0\phi_0\sigma_0\left[\frac{1}{E_\nu}\right]^{1.33}_{20} \quad (7)$$

where $n_0 = 6 \cdot 10^{32}$ nucleons/kt. Taking the integral limits between 1.33 and 20 GeV we find 3.30 events/(kt ster y). This number is in rough agreement with Super-K which sees 1053 multi-GeV

events ($E_\nu > 1.33$ GeV) in a 33 kt y exposure and 4π steradians i.e 2.54 events/(kt ster y) [6]. Their rate is somewhat smaller than the calculation because it cannot contain muons above 8 Gev/c and, of course, due to oscillation losses. The spherical 1 Mt AQUA-RICH detector instrumented from 0^0 to 70^0 and 110^0 to 180^0 ($\Delta\Omega \approx 8\pi/3$ ster) would detect about 27 650 events/y ($\approx$ 3/h).

3.2. Resolution and sensitivity

We consider interactions of neutrinos ν and antineutrinos $\bar{\nu}$ with a nucleon N via the process $\nu(\bar{\nu}) + N- > l^-(l^+) + p + n\pi^\pm$ with production of a lepton $l^\pm$, a proton p and $n \geq 0$ charged pions $\pi^\pm$ (no π^0's). We assume that AQUA-RICH measures the produced lepton, proton and hadron energies (E_l,E_p,E_π) with errors (σ_{E_l},σ_{E_p},σ_{E_π}) and momenta ($\boldsymbol{p}_\mathrm{l}$, $\boldsymbol{p}_\mathrm{p}$, $\boldsymbol{p}_\pi$) with direction errors ($\sigma_{\theta_\mathrm{l}}$,$\sigma_{\theta_\mathrm{p}}$,$\sigma_{\theta_\pi}$). Energy and momentum conservation require

$$E_\nu = E_\mathrm{l} + E_\mathrm{p} + E_\pi - M_N,$$

$$\boldsymbol{p}_\nu = \boldsymbol{p}_\mathrm{l} + \boldsymbol{p}_\mathrm{p} + \boldsymbol{p}_\pi. \tag{8}$$

The oscillation probability for ν_μ- $> \nu_\mu$ is

$$P_{\mu\mu} = 1 - \sin^2 2\theta \sin^2\left(\frac{\Delta m^2 L}{4\hbar c E_\nu}\right) \tag{9}$$

where E_ν is obtained experimentally via Eq. (8) by measuring the lepton, proton and pion total energies ($1/4\hbar c = 1.27$ GeV/eV^2 km). Events with electron or gamma showers are excluded. Atmospheric neutrinos have an earth pathlength $L = -D\cos\Theta$ where the earth's diameter $D = 12\,732$ km and Θ is the neutrino zenith angle (upward neutrinos have $\Theta > 90^0$). This is obtained from the scalar product of Eq. (8) with the earth unit radial vector (i.e the vertical) thus

$$\cos\Theta = \frac{p_{lz} + p_{\mathrm{p}z} + p_{\pi z}}{E_\nu} \tag{10}$$

The appearance probability for $\nu_\mu \to \nu_\alpha$ is $P_{\mu\alpha} = 1 - P_{\mu\mu}$ where $\alpha = e,\tau$ or s (for sterile).

We define ωx as the argument of the sine function in Eq. (9) with $\omega \equiv 1.27\Delta m^2$ and $x \equiv L/E_\nu$. The error on x is

$$\frac{\sigma_x}{x} = \sqrt{\left(\frac{\sigma_L}{L}\right)^2 + \left(\frac{\sigma_{E_\nu}}{E_\nu}\right)^2} \tag{11}$$

but $L = -D\cos\Theta$ thus $\sigma_L/L = \tan\Theta\sigma_\Theta$ and so in terms of the measured variables (Θ,E_ν)

$$\frac{\sigma_x}{x} = \sqrt{(\tan\Theta\ \sigma_\Theta)^2 + \left(\frac{\sigma_{E_\nu}}{E_\nu}\right)^2} \equiv R \tag{12}$$

thus $\sigma_x = xR$ where R is the detector fractional resolution (measuring large x is difficult because σ_x scales as x). To measure the $\sin^2\omega x$ function of Eq. (9) requires that it be sampled at least once between peak and valley thus the x error σ_x must be $\leq \pi/4\omega$. Combining with Eq. (12) leads to the condition

$$x \leq x_0 \equiv \frac{\pi}{4R\omega} = \frac{0.62 - (\mathrm{km} - \mathrm{eV}^2)/\mathrm{GeV}}{R\Delta m^2} \tag{13}$$

and for $\Delta m^2 = 3\times10^{-3}$ eV^2 (the central value of the Super-K experiment [6]) gives $x_0 \approx$ (207 km/GeV)/R.

3.2.1. Event simulation

To observe these effects, a large detector with good resolution is required in order to obtain a sufficient data sample in a reasonable time. This is illustrated in Figs. 3a–c where 15 000 upward and 15 000 downward atmospheric ν_μ events have been simulated (1 y of data in 1 Mt AQUA-RICH). Only events with an above threshold muon, proton and 0, 1 or 2 charged pions are retained (events with π^0s are excluded). Each particle of the event is assumed to be measured with resolutions $\sigma_E/E = (0\%, 5\%, 10\%)$ in energy and $\sigma_\theta = (0, 6, 6)$ mrad in direction, respectively. The overall resolution on neutrino energy E_ν and earth pathlength $L = -D\cos\Theta$ is obtained from Eq. (8), adding in quadrature the errors due to the individual particles. Fig. 3a shows the upward events (solid histogram) and the downward events (dotted histogram) versus L/E_ν for perfect particle energy and angle resolutions. Many oscillation periods can be clearly discerned for all Δm^2 and all L/E_ν but at $\Delta m^2 = 10^{-4}$ eV^2 only one half-period is available. Fig. 3b shows the same events with individual particle resolutions

$\sigma_E/E = 5\%$ and $\sigma_\theta = 6$ mrad. Fig. 3c shows again these events with $\sigma_E/E = 10\%$ and $\sigma_\theta = 6$ mrad.

3.2.2. A good detector

For a good detector ($R = 0.05$) (see Fig. 3b), events with $x = L/E_\nu \leq 4133$ km/GeV are useful for disappearance $\Delta m^2 \approx 3.10^{-3}\,\mathrm{eV}^2$ moreover, since $L = (-\cos\Theta)12732$ km, only events with $E_\nu = (-\cos\Theta)3.1$ GeV contribute to establish the oscillation pattern. To maintain the good R resolution, only events with $(0.34 < -\cos\Theta < 1)$ can be used otherwise R starts to be dominated by the angle error σ_Θ, hence $E_\nu > (1.1 - 3.1)$ GeV. Consequently, to establish oscillations, a good detector can use about 60% of the upward atmospheric flux from 1.33 to 20 GeV/c, otherwise the oscillations are washed out (compare Fig. 3a and c).

Surprisingly, it is easier to measure small $\Delta m^2(10^{-4}\,\mathrm{eV}^2)$ than large $(10^{-2}\,\mathrm{eV}^2)$ because oscillations are faster at low Δm^2 (see Fig. 3a). The lower limit $\Delta m^2 \approx 10^{-4}\,\mathrm{eV}^2$ occurs because, here, only the first peak to valley region can be sampled due to the limited size of the earth [i.e $\omega x \leq 0.77(\pi/2)$ for $L = 12732$ km and $E \geq 1.33$ GeV].

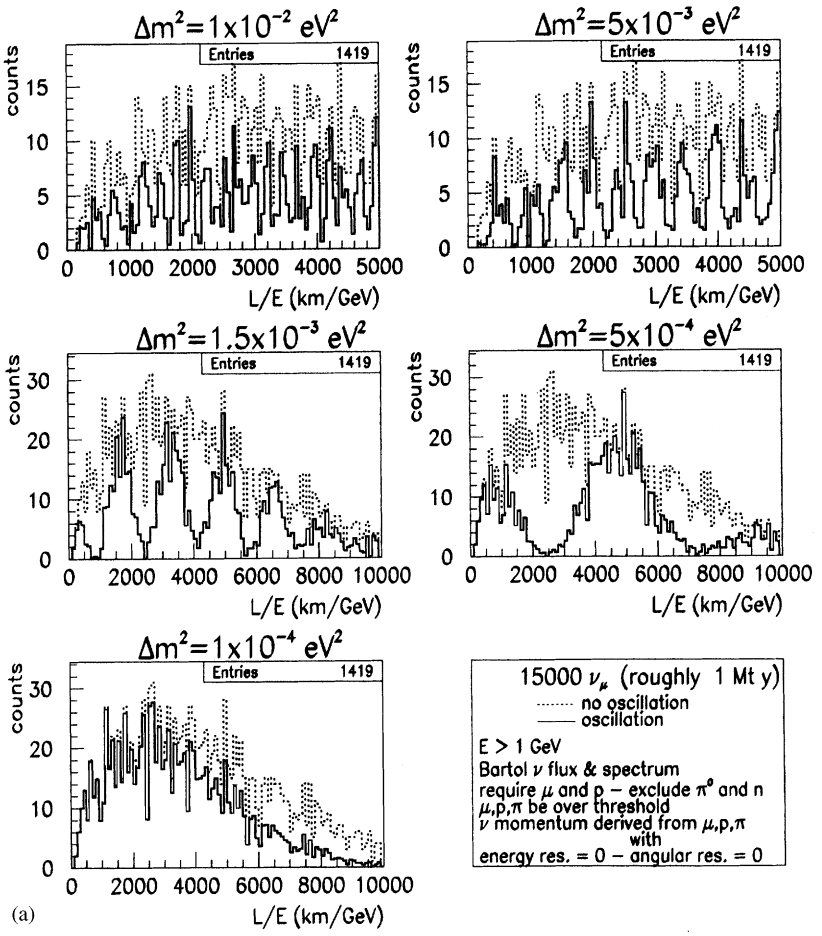

Fig. 3. (a) A simulated 1 Mt y sample of AQUA-RICH data for π steradian upward (solid line) or downward (dotted lines) atmospheric neutrino events with $E_\nu = 1$ to 20 GeV/c versus L/E_ν for oscillation parameters $\sin^2 2\,\theta = 1$ and labeled values of Δm^2. Accepted events required a muon and proton be detected (and 0, 1 or 2 charged pions but no π^0's). The imposed track energy and direction resolutions are $\sigma_E/E = 0, \sigma_{\theta x} = \sigma_{\theta y} = 0$ mrad, respectively.

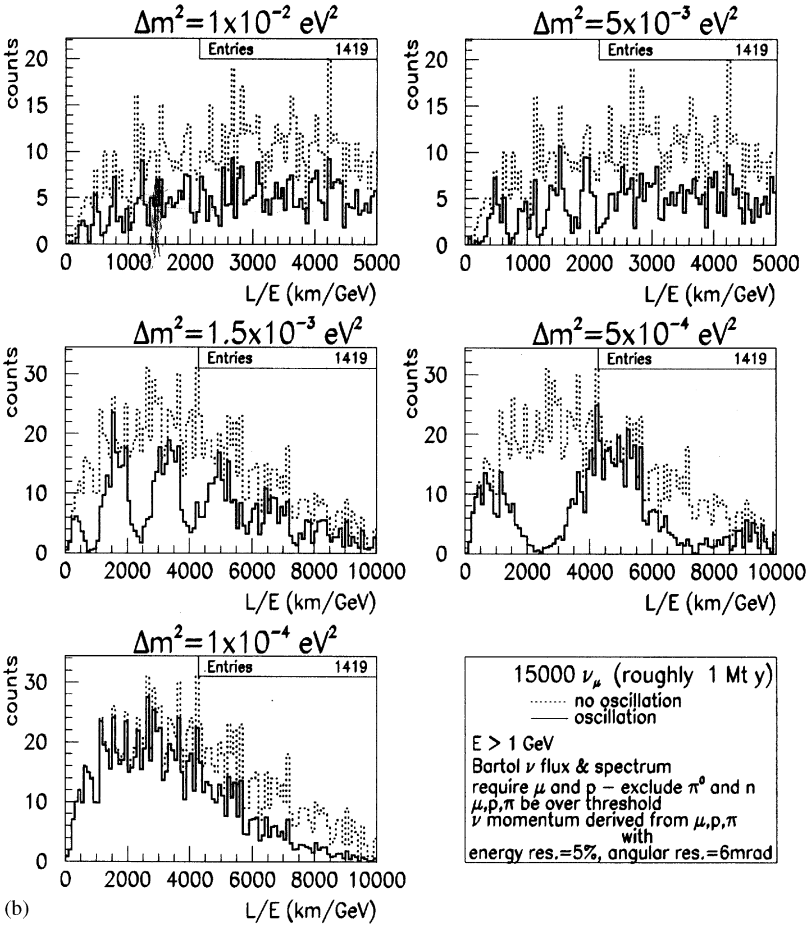

Fig 3. (b). Same as Fig. 3a except that the track energy and direction resolutions are $\sigma_E/E = 0.05, \sigma_{\theta x} = \sigma_{\theta y} = 6$ mrad, respectively.

For large $\Delta m^2 = 10^{-2}\,\mathrm{eV}^2$ and $R = 0.05$ then $x \leq 1240$ km/GeV consequently $E_\nu >$ (3.5–10.3) GeV thus only 14% of the atmospheric flux is useful. If the resolution worsens to $R = 0.1$ then $x \leq 620$ km/GeV and $E_\nu = (7.0–20.5)$ GeV then only 3% of the flux would be effective. Here, the first oscillation peak at $L/E_\nu \approx 400$ km/GeV, observable if $R = 0.05$, washes out if $R = 0.1$ (compare Fig. 3b and 3c).

In Fig. 3b ($\sigma_E/E = 5\%, \sigma_\theta = 6$ mrad) and for $\Delta m^2 = (100, 50, 15)10^{-4}\,\mathrm{eV}^2$ only (3, 4, 3) oscillation periods can be seen before the patterns wash out while at lower Δm^2 there is no loss of peaks. Eq. (13) predicts washout at $x = L/E_\nu = (1260, 2520, 8300)$ km/GeV, repectively, in good agreement with the simulation.

In Fig. 3c ($\sigma_E/E = 10\%, \sigma_\theta = 6$ mrad) and for $\Delta m^2 = (100, 50, 15, 5)10^{-4}\,\mathrm{eV}^2$ only (0, 1, 3, 2) oscillation peaks are seen whereas at $\Delta m^2 = 1 \times 10^{-4}\,\mathrm{eV}^2$ there is no loss of resolution. Eq. (12) predicts washout at $x = L/E_\nu = (630, 1260, 4150, 12600)$ km/GeV, repectively, again in good agreement with simulation.

3.2.3. A bad and a modest detector

For a bad detector ($R = 0.4$) only events with $x = L/E_\nu \leq 517$ km/GeV are effective $\Delta m^2 \gtrsim 3.10^{-3}\,\mathrm{eV}^2$ hence $E_\nu \geq (-\cos\Theta)24.6$ GeV and $E_\nu >$ (8.4–24.6)

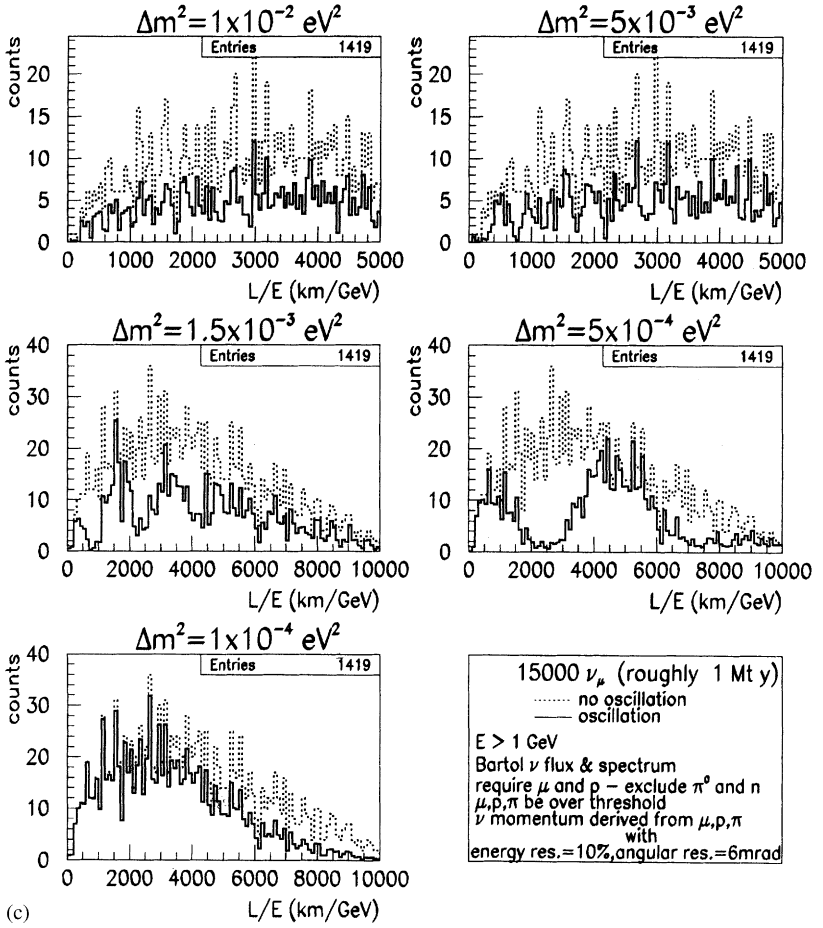

Fig. 3. (c). Same as Fig. 3a except that the track energy and direction resolutions are $\sigma_E/E = 0.10, \sigma_{\theta x} = \sigma_{\theta y} = 6$ mrad, respectively.

GeV which represents only 2% of the flux whereas a modest detector ($R = 0.2$) uses only about 10% of the atmospheric flux.

3.2.4. Detector generalities and conclusions

Good resolution is required in order to resolve the oscillation peaks at high Δm^2 and efficiently utilize the atmospheric flux to detect oscillations. A detector which measures both upward ($110^0 < \Theta < 180^0$) and downward ($0^0 < \Theta < 70^0$) events is self-normalizing and the result is independent of the neutrino flux. A detector which measures only upward events sees the disappearance effect modulated by the neutrino flux envelope however, the oscillations are still quite visible (see solid histograms in Fig. 3). It is clear from Eq. (12) that the region from $80^0 < \Theta < 100^0$ is not very useful because $\tan\Theta$, hence R, becomes large. In addition, the region $E_\nu < 1.33$ GeV is not useable because the recoil proton is below threshold moreover the Fermi momentum of struck nucleon limits both σ_{E_ν} and σ_θ.

We conclude that 1 Mt AQUA-RICH with $R \approx 0.05$ can confirm (or negate) the Super-K data and precisely determine Δm^2 from (100 to 1)10^{-4} eV^2 and large ($\sin^2 2\theta$).

3.3. Appearance of Tau or Sterile neutrinos

We simulated 7500 upward atmospheric neutrino interactions in water in the interval $0.5 < -\cos\Theta < 1$ i.e 0.5 y of AQUA-RICH data. We define CC events as those with an above threshold muon and proton and NC events as those without a muon. We chose events with $E_\nu > 10$ GeV and consider three cases:

(i) no oscillations;
(ii) oscillation $\nu_\mu -> \nu_\tau$;
(iii) oscillation $\nu_\mu -> \nu_s$.

In cases (ii) and (iii) the oscillation parameters were ($\Delta m^2 = 5 \times 10^{-3}$, $\sin^2 2\theta = 1$). For $L > 6366$ km and $10 < E_\nu < 20$ GeV then $\omega L \approx 3$ hence most ν_μ will have oscillated. We find

(i) CC + NC = 304 ± 17, NC/CC = 0.12 ± 0.02;
(ii) CC + NC = 224 ± 15, NC/CC = 0.60 ± 0.08;
(iii) CC + NC = 139 ± 12, NC/CC = 0.17 ± 0.04.

The three hypotheses are clearly discriminated.

4. Shielding of the 1 Mt sphere

Operation of AQUA-RICH, even in the full flux of downward cosmic muons, will be possible because Cherenkov light is fast and directional and HPDs have good timing characteristics. The calculated rate of downward muons in unshielded 1 Mt AQUA-RICH is 7 MHz but with 50 m of water shielding, which stops muons ≤ 10 GeV, the rate is reduced to 230 kHz, i.e one event every 4300 ns. For an HPD time resolution considerably < 1 ns, this rate should cause no trouble. In addition, the HPD occupancy will be negligible because of the large number of pixels (2.1 M) and the excellent multi-photon sensitivity of each pixel.

Cherenkov photons produced by downward cosmic muons would not be seen by the upper mHPDs but would be detected by the upper dHPDs to form a proximity focused-filled ring. These have, for any given number of photon hits, a hit density much less than for mirror-focused rings. Requiring hits to be concentrated on a smaller number of dHPDs will strongly discriminate against downward muons. Moreover, this can be done on the trigger level so as to limit the number of recorded events.

Upward tracks of length L(in m) will have about $230 L\varepsilon_g\varepsilon_a$ hits on mHPDs and $460 L\varepsilon_g\varepsilon_a$ hits on dHPDs but these will occur $t_0 = < q > n/c \approx 140$ ns later. Therefore, we will require the (n_m) hits on mHPDs to occur at time $t_m \pm \Delta t_m$ and the (n_d) hits on dHPDs to occur at time $t_d \pm \Delta t_d$ where $2\Delta t_m (2\Delta t_d)$ is the width of the mirror (detector) coincidence gate. The chosen minimum track length L will determine n_m,n_d. A true upward track will satisfy the condition $t_d - t_m > t_0 - \Delta t_m - \Delta t_d > 0$. Applying this temporal condition at the event trigger level will powerfully discriminate against downward muons.

Finally, in order that an event to be accepted as a valid neutrino interaction, we will require that at least two imaged rings have the same vertex well inside the water volume. This will be done off-line since it necessitates pattern recognition and reconstruction which cannot be done at the trigger level. As stated above, occupancy of the HPDs should not be a problem.

Recently, the AMANDA antarctic ice experiment [7] has reported a reduction of the downward cosmic flux by a factor 10^5 by requiring tracks to have the timing properties of an upward muon. Each track has about 20 PM hits on a vertical string with PMs separated by 20 m. They required ≥ 5 PM hits in a $(-15/+25)$ ns time window (wide because scattering in the ice). Even so, they were able to reject 10^5 downward muons as upward muon candidates. For HPDs with time resolution $\sigma_\tau < 1$ ns and 80–100 hits in an appropriately narrow time window, it is clear that rejections greater than the required factor of 10^{11} can be achieved.

5. Track and Cherenkov angle reconstruction

We consider an ZXY coordinate system (Fig. 4) fixed on earth with origin at the mirror center of curvature $C(z = x = y = 0)$ and Z vertical, X east and Y north. The PQR coordinate system is fixed to the particle direction vector with P along the track and Q and R perpendicular to the track, defined so that as $P \to Z$ then $R \to X$ and $Q \to Y$.

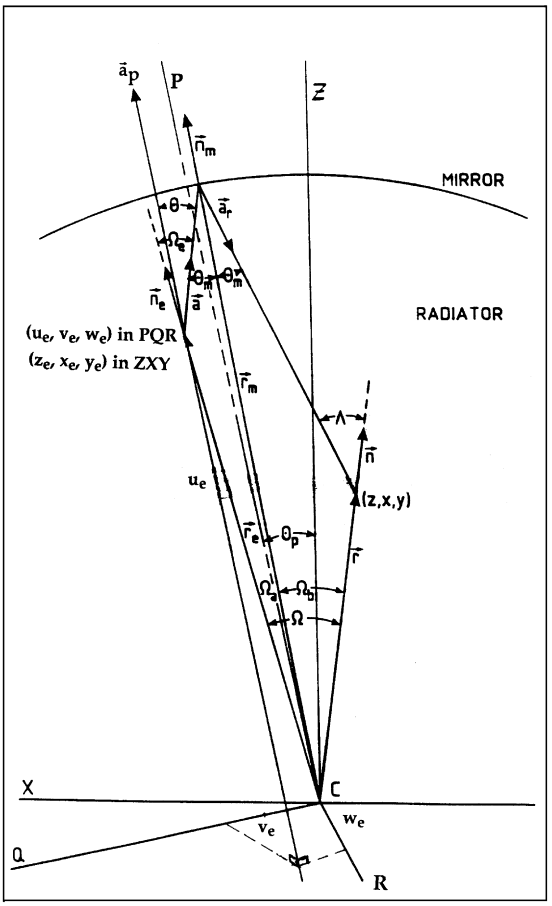

Fig. 4. The geometry of a mirror focused ring image defined by the mirror center of curvature C and the ZXY axes with origin at C and unit vectors ($\boldsymbol{k},\boldsymbol{i},\boldsymbol{j}$) fixed in space. The PQR axes with origin at C are defined so that P is parallel and Q and R are normal to the track with unit vectors ($\boldsymbol{a}_p,\boldsymbol{b}_p,\boldsymbol{c}_p$). The photon emission point is (z_e,x_e,y_e) in the ZXY system and (u_e,v_e,w_e) in the PQR system. The photon detection point is (z,x,y) in the ZXY system and (u,v,w) in the PQR system.

The unit vectors along (Z,X,Y) are ($\boldsymbol{k}$, $\boldsymbol{i}$, $\boldsymbol{j}$) and along (P,Q,R) are ($\boldsymbol{a}_p$, $\boldsymbol{b}_p$, $\boldsymbol{c}_p$).

5.1. Impact parameter, vertex and emission point vectors and Cherenkov angle

The unit vector $\boldsymbol{a}_p$ along the track, parallel to P has ZXY components

$$\boldsymbol{a}_p = a_{pz}\boldsymbol{k} + a_{px}\boldsymbol{i} + a_{py}\boldsymbol{j}$$

$$a_{pz} = \cos\theta_p$$

$$a_{px} = \sin\theta_p\cos\phi_p$$

$$a_{py} = \sin\theta_p\sin\phi_p. \tag{14}$$

The unit vector $\boldsymbol{b}_p$ along Q has components in ZXY

$$\boldsymbol{b}_p = b_{pz}\boldsymbol{k} + b_{px}\boldsymbol{i} + b_{py}\boldsymbol{j}$$

$$b_{pz} = -a_{px}$$

$$b_{px} = \sin^2\phi_p + \cos\theta_p\cos^2\phi_p \equiv \varepsilon_x$$

$$b_{py} = (\cos\theta_p - 1)\cos\phi_p\sin\phi_p \equiv \eta. \tag{15}$$

The unit vector $\boldsymbol{c}_p = \boldsymbol{a}_p x \boldsymbol{b}_p$ along R is normal to $\boldsymbol{a}_p$ and $\boldsymbol{b}_p$ with ZXY components

$$\boldsymbol{c}_p = c_{pz}\boldsymbol{k} + c_{px}\boldsymbol{i} + c_{py}\boldsymbol{j}$$

$$c_{pz} = -a_{py}$$

$$c_{px} = \eta$$

$$c_{py} = \cos^2\phi_p + \cos\theta_p\sin^2\phi_p \equiv \varepsilon_y. \tag{16}$$

The specific choice of QR is made such that as $\theta_p \to 0$ then $\boldsymbol{a}_p \to \boldsymbol{k}, \boldsymbol{b}_p \to \boldsymbol{i}, \boldsymbol{c}_p \to \boldsymbol{j}$.

The particle production (neutrino interaction) vertex $\boldsymbol{r}_v$ has ZXY components (z_v,x_v,y_v) and PQR components (u_v,v_v,w_v) where

$$\boldsymbol{r}_v = z_v\boldsymbol{k} + x_v\boldsymbol{i} + y_v\boldsymbol{j} = u_v\boldsymbol{a}_p + v_v\boldsymbol{b}_p + w_v\boldsymbol{c}_p$$

$$u_v = \boldsymbol{r}_v\cdot\boldsymbol{a}_p$$

$$v_v = \boldsymbol{r}_v\cdot\boldsymbol{b}_p$$

$$w_v = \boldsymbol{r}_v\cdot\boldsymbol{c}_p. \tag{17}$$

The impact parameter $\boldsymbol{r}_{ip}$ is that vector normal to $\boldsymbol{a}_p$ which when added to a vector proportional to $\boldsymbol{a}_p$ gives the vertex vector $\boldsymbol{r}_v$ i.e

$$\boldsymbol{r}_{ip} = \boldsymbol{r}_v - (\boldsymbol{r}_v\cdot\boldsymbol{a}_p)\boldsymbol{a}_p = v_v\boldsymbol{b}_p + w_v\boldsymbol{c}_p \tag{18}$$

thus v_v and w_v are the impact parameters.

In ZXY the photon emission point is (z_e,x_e,y_e) i.e $\boldsymbol{r}_e = z_e\boldsymbol{k} + x_e\boldsymbol{i} + y_e\boldsymbol{j}$. In PQR the emission point is at distance u_{ve} along $\boldsymbol{a}_p$ from $\boldsymbol{r}_v$ hence

$$\boldsymbol{r}_e = \boldsymbol{r}_v + u_{ve}\boldsymbol{a}_p = u_e\boldsymbol{a}_p + v_e\boldsymbol{b}_p + w_e\boldsymbol{c}_p \tag{19}$$

where $u_e = u_v + u_{ve}, v_e = v_v, w_e = w_v$ and $r_e = \sqrt{(u_e^2 + v_e^2 + w_e^2)} = \sqrt{(z_e^2 + x_e^2 + y_e^2)}$. Note that the emission point coordinates (u_e,v_e) are constant

along a track and equal to the vertex impact parameters (u_v,v_v) whereas u_e varies along the track. Since the (z_e,x_e,y_e) coordinates are defined in ZXY they are obviously independent of (θ_p,ϕ_p). Note that a normal high energy physics tracker (a series of MWCs or Silicon planes) would directly measure the track parameters $\boldsymbol{r}_{ip}$ and $\boldsymbol{a}_p$ i.e $(u_v,v_v,\theta_p,\phi_p)$.

Eq. (19) gives (u_e,v_e,w_e) in terms of (z_e,x_e,y_e) and a matrix $A(\theta_p,\phi_p)$ i.e

$$\begin{pmatrix} u_e \\ v_e \\ w_e \end{pmatrix} = \begin{pmatrix} a_{pz} & a_{px} & a_{py} \\ -a_{px} & \varepsilon_x & \eta \\ -a_{py} & \eta & \varepsilon_y \end{pmatrix} \begin{pmatrix} z_e \\ x_e \\ y_e \end{pmatrix} \equiv A \begin{pmatrix} z_e \\ x_e \\ y_e \end{pmatrix} \tag{20}$$

with the inverse tranformation

$$\begin{pmatrix} z_e \\ x_e \\ y_e \end{pmatrix} = \begin{pmatrix} a_{pz} & -a_{px} & -a_{py} \\ a_{px} & \varepsilon_x & \eta \\ a_{py} & \eta & \varepsilon_y \end{pmatrix} \begin{pmatrix} u_e \\ v_e \\ w_e \end{pmatrix} \equiv B \begin{pmatrix} u_e \\ v_e \\ w_e \end{pmatrix} \tag{21}$$

In matrix notation $u_e = Az_e$ and $z_e = Bu_e$ where u_e and z_e are column vectors $(u_e,v_e,w_e)^T,(z_e,x_e,y_e)^T$. Note that $AB = 1$ hence $B = A^{-1} = A^T$ where T indicates transpose, i.e $(A^T)_{ij} = a_{ji}$.

The detection point vector $\boldsymbol{r} = r\boldsymbol{n}$ has components (z,x,y) in ZXY which are independent of (θ_p, ϕ_p) while (u,v,w) in the PQR system depend on (θ_p, ϕ_p) as

$$\boldsymbol{r} = z\boldsymbol{k} + x\boldsymbol{i} + y\boldsymbol{j} = u\boldsymbol{a}_p + v\boldsymbol{b}_p + w\boldsymbol{c}_p$$

$$u = Az$$

$$z = Bu. \tag{22}$$

Finally, the photon unit vector $\boldsymbol{a}$ has PQR components $a_e = (a_a = \cos\theta, a_b = \sin\theta\cos\phi, a_c = \sin\theta\sin\phi)^T$ independent of A. Its ZXY components depend on A via the equations

$$\boldsymbol{a} = a_a\boldsymbol{a}_p + a_b\boldsymbol{b}_p + a_c\boldsymbol{c}_p = a_z\boldsymbol{k} + a_x\boldsymbol{i} + a_y\boldsymbol{j}$$

$$a = Ba_e$$

$$a_e = Aa \tag{23}$$

with $a = (a_z,a_x,a_y)^T$ and $a^2 = a_e^2 = 1$.

Because the emitted photon plane containing $\boldsymbol{n}_e$ and $\boldsymbol{a}$ also contains C and because the mirror normal (at the reflection point) is also in this plane, thus the reflected photon will remain in this plane (see Fig. 4). This is expressed by the vector equation

$$\boldsymbol{n} = \mu\boldsymbol{n}_e + \nu\boldsymbol{a} \tag{24}$$

with μ and ν to be determined. We define the angles $(\Omega,\Omega_e,\Omega')$ by the dot products

$$\boldsymbol{n}\cdot\boldsymbol{n}_e \equiv \cos\Omega$$

$$\boldsymbol{a}\cdot\boldsymbol{n}_e \equiv \cos\Omega_e$$

$$\boldsymbol{a}\cdot\boldsymbol{n} \equiv \cos\Omega' \tag{25}$$

also shown in Fig. 4. Taking the dot product of Eq. (24) with each of $(\boldsymbol{a},\boldsymbol{n}_e,\boldsymbol{n})$ and solving the first two resultant equations for μ and ν gives

$$\mu = \frac{\sin\Omega'}{\sin\Omega_e}$$

$$\nu = \frac{\sin\Omega}{\sin\Omega_e}, \tag{26}$$

The third equation is satisfied if $\Omega' = \Omega_\varepsilon - \Omega$ however this is always true since the three vectors form a closed triangle. Note that Ω is found directly from experiment as

$$\cos\Omega = \boldsymbol{n}\cdot\boldsymbol{n}_e = \frac{zz_e + xx_e + yy_e}{rr_e} = \frac{uu_e + vv_e + ww_e}{rr_e}. \tag{27}$$

A normal tracker measures $(u_v, v_v, \theta_p, \phi_p)$ and the dHPD hit gives (z,x,y) hence $u = Az$ is known. The impact parameter part of the emission point is also known because $v_e = v_v$ and $w_e = w_v$. The emission point u_e along the the track is taken at the radiator midpoint, thus Ω is found from the 2nd equality of Eq. (27). This works well with trackers at accelerators, but without a tracker another strategy is required.

Assume for the moment that $(u_e,v_e,w_e,\theta_p,\phi_p)$ are known thus $z_e = Bu_e$ is also known and with the measured hit point (z,x,y), the first equality of Eq. (27) gives Ω. From the RICH geometry (see Fig. 4) we find $\Omega = \Omega_e + \Lambda - 2\theta_m$ which, with the sine law equalities $r_e\sin\Omega_e \equiv r_a = r_m\sin\theta_m = r\sin\Lambda$, becomes

$$\Omega = \Omega_e + \sin^{-1}\left(\frac{r_a}{r}\right) - 2\sin^{-1}\left(\frac{r_a}{r_m}\right) \tag{28}$$

thus we obtain Ω_e from Ω by numerical inversion of Eq. (28) and μ,ν from Eq. (26). Geometrically, r_a

represents the photon impact parameter. Then solving Eq. (24) for $\boldsymbol{a}$ gives

$$\boldsymbol{a} = \left(\frac{1}{v}\right)\boldsymbol{n} - \left(\frac{\mu}{v}\right)\boldsymbol{n}_{\mathrm{e}} = \left(\frac{\sin\Omega_{\mathrm{e}}}{\sin\Omega}\right)\boldsymbol{n} - \left[\frac{\sin(\Omega_{\mathrm{e}}-\Omega)}{\sin\Omega}\right]\boldsymbol{n}_{\mathrm{e}}. \tag{29}$$

Since the components of $\boldsymbol{a}$ in PQR are ($a_a = \cos\theta, a_b = \sin\theta\cos\phi, a_c = \sin\theta\sin\phi$) we find the explicit reconstruction equations

$$\cos\theta = \left(\frac{\sin\Omega_{\mathrm{e}}}{\sin\Omega}\right)\left(\frac{u}{r}\right) - \left[\frac{\sin(\Omega_{\mathrm{e}}-\Omega)}{\sin\Omega}\right]\left(\frac{u_{\mathrm{e}}}{r_{\mathrm{e}}}\right)$$

$$\sin\theta\cos\phi = \left(\frac{\sin\Omega_{\mathrm{e}}}{\sin\Omega}\right)\left(\frac{v}{r}\right) - \left[\frac{\sin(\Omega_{\mathrm{e}}-\Omega)}{\sin\Omega}\right]\left(\frac{v_{\mathrm{e}}}{r_{\mathrm{e}}}\right)$$

$$\sin\theta\sin\phi = \left(\frac{\sin\Omega_{\mathrm{e}}}{\sin\Omega}\right)\left(\frac{w}{r}\right) - \left[\frac{\sin(\Omega_{\mathrm{e}}-\Omega)}{\sin\Omega}\right]\left(\frac{w_{\mathrm{e}}}{r_{\mathrm{e}}}\right). \tag{30}$$

Thus θ and ϕ are obtained from (z,x,y),$(u_{\mathrm{e}},v_{\mathrm{e}},w_{\mathrm{e}})$ and $A(\theta_{\mathrm{p}},\phi_{\mathrm{p}})$. Of course (u,v,w) are obtained via the rotation matrix $u = Az$ whereas $(u_{\mathrm{e}},v_{\mathrm{e}},w_{\mathrm{e}})$ are determined either by a normal tracker or HPD timing. This algorithm is general, it works for any detector surface and removes all but intrinsic aberrations of the image.

5.2. Measurements of time and the time constraint from dHPD hits

The long muon track is easily recognized in AQUA-RICH by the large number of focused hits on the dHPDs. The corresponding photon emission point $(z_{\mathrm{e}},x_{\mathrm{e}},y_{\mathrm{e}})$ can be determined by measuring time. The image is defined by an array of N image points (z,x,y) on the dHPDs each with an associated photon arrival time $t \pm \sigma_t$. The photon pathlengths are l_1 between the emission point $\boldsymbol{r}_{\mathrm{e}}$ and the mirror reflection point $\boldsymbol{r}_{\mathrm{m}}$ and l_2 from $\boldsymbol{r}_{\mathrm{m}}$ to the photon detection point $\boldsymbol{r}$. These are found from the Fig. 4 geometry as

$$l_1 = r_{\mathrm{m}}\cos\theta_{\mathrm{m}} - r_{\mathrm{e}}\cos\Omega_{\mathrm{e}} = r_{\mathrm{d}} - r_{\mathrm{b}}$$

$$l_2 = r_{\mathrm{m}}\cos\theta_{\mathrm{m}} - r\cos\Lambda = r_{\mathrm{d}} - r_{\mathrm{c}}$$

where

$$r_{\mathrm{d}} \equiv r_{\mathrm{m}}\cos\theta_{\mathrm{m}} = \sqrt{r_{\mathrm{m}}^2 - r_{\mathrm{a}}^2}$$

$$r_{\mathrm{c}} \equiv r\cos\Lambda = \sqrt{r^2 - r_a^2}$$

$$r_{\mathrm{b}} \equiv r_{\mathrm{e}}\cos\Omega_{\mathrm{e}} = \sqrt{r_{\mathrm{e}}^2 - r_{\mathrm{a}}^2}$$

$$r_{\mathrm{a}} \equiv r_{\mathrm{e}}\sin\Omega_{\mathrm{e}} \tag{31}$$

with Ω_{e} from Eq. (28). The total photon pathlength is

$$l \equiv l_1 + l_2 = 2r_{\mathrm{d}} - r_{\mathrm{c}} - r_{\mathrm{b}} = \frac{ct_{\mathrm{t}}}{n} \tag{32}$$

where t_t is the photon transit time from emission to detection. Eq. (32) is independent of particle direction $(\theta_{\mathrm{p}},\phi_{\mathrm{p}})$ and depends only on r_{e} and r_{a}. Clearly, the arrival time on the dHPD $t = t_{\mathrm{v}} + (u_{\mathrm{ve}}/\beta c) + t_{\mathrm{t}}$ which, when combined with Eq. (32) gives the time constraint

$$f_{\mathrm{t}} \equiv t - t_{\mathrm{v}} - \frac{n}{c}[2r_{\mathrm{d}} - r_{\mathrm{c}} - r_{\mathrm{b}} + (u_{\mathrm{e}} - u_{\mathrm{v}})/\beta n] = 0. \tag{33}$$

Thus, if t_{v} and u_{v} are known, then Eq. (33) provides a constraint on u_{e},β and r_{a}. This constraint can be combined with the space constraint to determine u_{e} (see below).

5.3. The space constraint from dHPD hits

We combine Eqs. (27) and (28) to obtain a second constraint (the space constraint f_s) which is a function of $(r_{\mathrm{a}}^2,u,v,w,u_{\mathrm{e}},v_{\mathrm{e}} = v_{\mathrm{v}}$ and $w_{\mathrm{e}} = w_{\mathrm{v}})$ i.e

$$f_s \equiv r_{\mathrm{m}}^2(u_{\mathrm{i}}u_{\mathrm{e}} + vv_{\mathrm{e}} + ww_{\mathrm{e}}) - (r_{\mathrm{m}}^2 - 2r_{\mathrm{a}}^2)(r_{\mathrm{b}}r_{\mathrm{c}} - r_{\mathrm{a}}^2) + 2r_{\mathrm{d}}(r_{\mathrm{b}} + r_{\mathrm{c}})r_{\mathrm{a}}^2 = 0. \tag{34}$$

This equation can also be obtained as the quadratic sum of Eq. (30) components, i.e the emitted photon modulus $a_{\mathrm{e}}^2 = a_{\mathrm{a}}^2 + a_{\mathrm{b}}^2 + a_{\mathrm{c}}^2 = 1$. We note that r_{b} is the only element in Eq. (34) which depends on

r_e thus solving for r_b gives the equation

$$r_b = \sqrt{r_e^2 - r_a^2} = \sqrt{u_e^2 + \alpha} = \frac{Eu_e + F}{D}$$

with

$$D \equiv r_m^2 r_c + 2r_a^2(r_d - r_c)$$

$$E \equiv r_m^2 u$$

$$F \equiv r_m^2(vv_v + ww_v) + r_a^2(r_m^2 - 2r_a^2 - 2r_c r_d)$$

$$\alpha \equiv v_v^2 + w_v^2 - r_a^2. \tag{35}$$

Apart from the given fixed parameters $(r_m,r,v_v,w_v,\theta_p,\phi_p)$,$D$ and α are functions only of r_a whereas $E = E(u)$ and $F = F(r_a,u,v,w)$ however since $u = Az$ and z is the known hit point thus D,α and F depend only on r_a. Note that Eq. (35) is quadratic in u_e and its solution

$$u_e = \frac{EF + D\sqrt{F^2 - \alpha(D^2 - E^2)}}{D^2 - E^2} = u_e(r_a) \tag{36}$$

is a function only of r_a. By combining the space (Eq. (36)) and time (Eq. (33)) constraints we obtain an equation which is a function only of β and r_a, i.e

$$\frac{c}{n}(t - t_v) = 2r_d - r_c - \frac{F}{D} + \frac{u_v}{\beta n} - \left(\frac{1}{\beta n} + \frac{E}{D}\right)\frac{EF + D\sqrt{F^2 - \alpha(D^2 - E^2)}}{D^2 - E^2}. \tag{37}$$

For $\beta = 1$ we vary r_a to find the zero of Eq. (37). Inserting this value of r_a into Eq. (36) gives a good estimate for u_e (not exact since β may not be exactly 1). Inserting this u_e into Eq. (30) then gives the reconstructed Cherenkov emission angles (θ,ϕ).

For long tracks (muons) this procedure is necessary otherwise the emission point error $\sigma_\theta(u_e)$, rather than $\sigma_\theta(ms)$, will dominate the total ring width σ_θ. It also improves σ_θ for a short tracks if they arise from the same vertex.

5.4. Finding the vertex 4 vector and particle direction vector from mHPD hits

A long muon track in AQUA-RICH can also be recognized from mHPD hits because, if it reaches the mirror surface, it produces a filled in circle (i.e a blob). If it does not reach the mirror surface it produces a proximity focused ring. Both cases are covered by the present treatment.

5.5. Vertex point and time from mHPD hits

Using the outer (later in time) mHPD hit points gives essentially the vertex point and time (z_v,x_v,y_v,t_v). These also determine the muon direction cosines (a_{pz},a_{px},a_{py}) hence the rotation matrix A. Since the mirror hit points are caused by photons, they must obey the spherical wave constraint f (even though they populate a cone) thus

$$f_i \equiv (z_i - z_v)^2 + (x_i - x_v)^2 + (y_i - y_v)^2 - (t_i - t_v)^2(c/n)^2 = 0 \tag{38}$$

where the subscript i represents the ith mHPD hit point ($i = 1,2,\ldots,N$). When discussing mirror hits we drop the subscript m and the factor c/n, i.e all times will be expressed as distances. Translating the origin of the coordinate system to the "center of hits" guarantees that $\bar{z} = \bar{x} = \bar{y} = \bar{t} = 0$ thus, averaging this constraint over the N mirror hits requires

$$\overline{f} = \overline{z^2} + \overline{x^2} + \overline{y^2} - \overline{t^2} + z_v^2 + x_v^2 + y_v^2 - t_v^2 \equiv \overline{s^2} + s_v^2 = 0$$

$$\overline{s^2} \equiv \overline{z^2} + \overline{x^2} + \overline{y^2} - \overline{t^2}$$

$$s_v^2 \equiv z_v^2 + x_v^2 + y_v^2 - t_v^2 \tag{39}$$

thus constraining s_v^2. We now define a χ^2 with equal space errors i.e $\sigma_z = \sigma_x = \sigma_y$ thus

$$\chi^2 = \sum_i^N \frac{f_i^2}{\sigma_f^2}$$

$$\sigma_f^2 = 4[(z_i - z_v)^2\sigma_z^2 + (x_i - x_v)^2\sigma_x^2 + (y_i - y_v)^2\sigma_y^2 + (t_i - t_v)^2\sigma_t^2]$$

$$\sigma_f^2 \cong 4(t_i - t_v)^2(\sigma_z^2 + \sigma_t^2). \tag{40}$$

Assuming that σ_f^2 is constant with respect to variations in (z_v,x_v,y_v,t_v) and requiring $\partial\chi^2/\partial z_v = 0, \partial\chi^2/\partial x_v = 0, \partial\chi^2/\partial y_v = 0, \partial\chi^2/\partial t_v = 0$ results in four equations, i.e

$$\begin{pmatrix} \overline{z^2}+\overline{f/2} & \overline{zx} & \overline{zy} & \overline{-zt} \\ \overline{zx} & \overline{x^2}+\overline{f/2} & \overline{xy} & \overline{-xt} \\ \overline{zy} & \overline{xy} & \overline{y^2}+\overline{f/2} & \overline{-yt} \\ \overline{zt} & \overline{xt} & \overline{yt} & \overline{-t^2}+\overline{f/2} \end{pmatrix} \begin{pmatrix} z_v \\ x_v \\ y_v \\ t_v \end{pmatrix} = \frac{1}{2}\begin{pmatrix} \overline{zs^2} \\ \overline{xs^2} \\ \overline{ys^2} \\ \overline{ts^2} \end{pmatrix}. \tag{41}$$

These equations are linear if the constraint $\bar{f}=0$ is satisfied otherwise, they are cubic. To obtain stable and meaningful solutions of the linear equations it was necessary to use the method of Gaussian elimination with partial pivoting. Of course, the assumption that σ_f^2 is constant is suspect and a true minimization of Eq. (40) without this anzatz should be attempted. This has not been done. An iterative solution, starting with $\bar{f}=0$ and increasing the diagonal elements by the value of $(\bar{f}/2)$ found in the preceeding iteration, failed to converge.

5.6. Lagrangian multipliers

The constraint $\bar{f}=0$ may be imposed by the method of Lagrangian multipliers. We define the Lagrangian function (again neglecting the error denominator) as

$$L \equiv \sum_i f_i^2 + 4\lambda\overline{s^2}\bar{f} \tag{42}$$

where the Lagrangian multiplier, λ, is treated as an unknown to be determined along with (z_v,x_v,y_v,t_v) by minimization of L. Requiring that $\partial L/\partial\lambda = 0$ guarantees that the contraint $\bar{f}=0$ and requiring $\partial L/\partial\zeta_i = 0$ (for $\zeta_i = z_v,x_v,y_v,t_v$) gives again four linear equations but now with a term $\lambda\overline{s^2}$ added to the diagonals of the matrix, i.e

$$\begin{pmatrix} \overline{z^2}+\lambda\overline{s^2} & \overline{zx} & \overline{zy} & \overline{-zt} \\ \overline{zx} & \overline{x^2}+\lambda\overline{s^2} & \overline{xy} & \overline{-xt} \\ \overline{zy} & \overline{xy} & \overline{y^2}+\lambda\overline{s^2} & \overline{-yt} \\ \overline{zt} & \overline{xt} & \overline{yt} & \overline{-t^2}+\lambda\overline{s^2} \end{pmatrix} \begin{pmatrix} z_v \\ x_v \\ y_v \\ t_v \end{pmatrix} = \frac{1}{2}\begin{pmatrix} \overline{zs^2} \\ \overline{xs^2} \\ \overline{ys^2} \\ \overline{ts^2} \end{pmatrix}. \tag{43}$$

It then suffices to solve the four linear equations varying the single variable λ to obtain minimum L and so obtain a solution $(z_{vs},x_{vs},y_{vs},t_{vs})$ which satisfies the constraint $\bar{f}=0$. Solutions for MC events plotted in the variables $z_{vs}-z_v, x_{vs}-x_v, y_{vs}-y_v$ and $t_{vs}-t_v$ show Gaussian distributions with tails.

5.7. Particle direction from mHPD hits

Again we consider the outer (late) hits on the mHPDs which come from the region of the vertex. To determine particle direction we consider the 3-vector r_i representing the ith mirror hit point. The vertex point components are r_{vi} hence the photon track of length l and direction a_i is simply given by the vector difference i.e $la_i = r_i - r_{vi}$. Taking the dot product with respect to particle direction gives $la_ia_{pi} = (r_i - r_{ei})a_{pi} = l\cos\theta$ (sum over repeated indices). The length l is found from the measured time difference $t_i - t_v$ and so the basic equation becomes $(r_i - r_{vi})a_{pi} = (t_i - t_v)\cos\theta$. Averaging over hits in the translated ZXY system, where $(\bar{z}=\bar{x}=\bar{y}=\bar{t}=0)$, gives $r_{vi}a_{pi} = t_v\cos\theta$ i.e $z_va_{pz} + x_va_{px} + y_va_{py} = t_v\cos\theta$ where (z_v,x_v,y_v,t_v) are solutions of Eq. (42). A second (obvious) additional constraint which must be satisfied is $a_{pi}a_{pi} = a_{pz}^2 + a_{px}^2 + a_{py}^2 = 1$.

Multiplying the basic equation by r_k and averaging over hits gives the set of linear equations $T_{ki}a_{pi} = V_k\cos\theta$ with tensor $T_{ki} = \overline{r_kr_i}$ and vector $V_k = \overline{r_kt}$. Thus we find the same 3×3 tensor elements as in Eq. (43) (i.e $T_{11} = \overline{z^2}, T_{12} = \overline{zx}, T_{13} = \overline{zy}, \ldots$) but with vector components $V_1 = \overline{zt}$, $V_2 = \overline{xt}$, $V_3 = \overline{yt}$.

5.8. Lagrangian multipliers

The problem here is to solve three linear equations with one linear and one quadratic constraint. We define a function L with two Lagrangian multipliers λ_1 and λ_2, i. e

$$L \equiv \sum_i g_i^2 + \lambda_1 \overline{s^2}(a_{pz}^2 + a_{px}^2 + a_{py}^2 - 1) + \lambda_2 \bar{s}\bar{g}$$

$$g_i = (z_i - z_v)a_{pz} + (x_i - x_v)a_{px} + (y_i - y_v)a_{py} - [(t_i - t_v)/n\beta]$$

$$\bar{g} = [t_v/n\beta] - z_v a_{pz} - x_v a_{px} - y_v a_{py} = 0$$

$$a_{pz}^2 + a_{px}^2 + a_{py}^2 - 1 = 0 \tag{44}$$

where $\bar{s} \equiv \sqrt{\bar{s}^2}$. Minimizing L with respect to a_{pz},a_{px},a_{py}, λ_1 and λ_2 we obtain three linear equations for a_{pz},a_{px},a_{py} which satisfy the two constraints, i.e

$$\begin{pmatrix} \overline{z^2} + z_v^2 + \lambda_1 \overline{s^2} & \overline{zx} + z_v x_v & \overline{zy} + z_v y_v \\ \overline{zx} + z_v x_v & \overline{x^2} + x_v^2 + \lambda_1 \overline{s^2} & \overline{xy} + x_v y_v \\ \overline{zy} + z_v y_v & \overline{xy} + x_v y_v & \overline{y^2} + y_v^2 + \lambda_1 \overline{s^2} \end{pmatrix}$$

$$\begin{pmatrix} a_{pz} \\ a_{px} \\ a_{py} \end{pmatrix} = \begin{pmatrix} (\overline{zt} + z_v t_v)/n\beta + \lambda_2 \bar{s} z_e \\ (\overline{xt} + x_v t_v)/n\beta + \lambda_2 \bar{s} x_e \\ (\overline{yt} + y_v t_v)/n\beta + \lambda_2 \bar{s} y_e \end{pmatrix}. \tag{45}$$

These equations are solved for $\beta = 1$ varying λ_1 and λ_2 to minimize L thus to obtain the solution vector (a_{pzs},a_{pxs},a_{pys}). This algorithm gives for a sample of MC events the reconstructed direction errors $\sigma_{\theta x} \approx \sigma_{\theta y} \approx 6$ mrad ($\tan\theta_x = a_{px}/a_{pz}$,$\tan\theta_y = a_{py}/a_{pz}$).

5.9. Finding both vertex 4 vector and particle direction from the mHPD hits points

Here we look for equations which use all the mirror hit points to determine the vertex 4 vector and the particle direction. These equation will allow simultaneous variation of (u_v,w_v,z_v,t_v) and (a_{pz},a_{px},a_{py}). The mirror hit point is given by the vector equations

$$\boldsymbol{r}_m = \boldsymbol{r}_e + l_1 \boldsymbol{a} = \boldsymbol{r}_v + u_{ve}\boldsymbol{a}_p + l_1 \boldsymbol{a}$$

$$u_m = \boldsymbol{r}_m \cdot \boldsymbol{a}_p = u_v + u_{ve} + l_1 \cos\theta$$

$$v_m = \boldsymbol{r}_m \cdot \boldsymbol{b}_p = v_v + 0 + l_1 \sin\theta \cos\phi$$

$$w_m = \boldsymbol{r}_m \cdot \boldsymbol{c}_p = w_v + 0 + l_1 \sin\theta \sin\phi \tag{46}$$

where $u_{ve} = (t_v - t_e)\beta c$ and $l_1 = (t_m - t_e)c/n$. We write explicitly the velocites because there are two different velocities i.e βc for the particle and c/n for the photon. Two components of Eq. (46) are used to eliminate t_e and ϕ leaving the single-constraint equation dropping the m subscript and again expressing time as length with water velocity $= c/n$

$$h_i \equiv v[(u_i - u_v) + n\beta(t_i - t_v)]^2 - \mu[(v_i - v_v)^2 + (w_i - w_v)^2] = 0 \tag{47}$$

with $\mu = (n\beta + 1/n\beta)^2 \approx 4.35$,$v = \sin^2\theta = 1 - 1/n^2\beta^2 \approx 0.44$ and with $\lambda = \mu + v = 3 + n^2\beta^2 \approx 4.79$. Expressing ($u$,$v$,$w$) in terms of the measured (z,x,y) mHPD hit points and the desired direction components (a_{pz},a_{px},a_{py}) via $u = Az$ thus the constraint becomes

$$\begin{aligned} h_i = {} & \lambda(a_{pz}^2 z_i^2 + a_{px}^2 x_i^2 + a_{py}^2 y_i^2 + 2a_{pz}a_{px}z_i x_i \\ & + 2a_{pz}a_{py}z_i y_i + 2a_{px}a_{py}x_i y_i) + v u_v^2 \\ & - \mu(r_m^2 + u_v^2 + v_v^2) + \beta^2 c^2 v(t_i^2 + t_v^2 - 2t_i t_v) \\ & + 2z_i[\mu(v_v b_{pz} + w_v c_{pz}) - v u_v a_{pz}] \\ & + 2x_i[\mu(v_v b_{px} + w_v c_{px}) - v u_v a_{pz}] \\ & + 2y_i[\mu(v_v b_{py} + w_v c_{py}) - v u_v a_{py}] \\ & + 2\beta c v[a_{pz}z_i t_i + a_{px}x_i t_i + a_{py}y_i t_i + u_v t_v \\ & - t_v(a_{pz}z_i + a_{px}x_i + a_{py}y_i) - u_v t_i] = 0 \end{aligned} \tag{48}$$

and its average

$$\begin{aligned} \bar{h} = {} & \lambda(a_{pz}^2 \overline{z^2} + a_{px}^2 \overline{x^2} + a_{py}^2 \overline{y^2} + 2a_{pz}a_{px}\overline{zx} \\ & + 2a_{pz}a_{py}\overline{zy} + 2a_{px}a_{py}\overline{xy}) + v u_v^2 \\ & - \mu(r_m^2 + u_v^2 + v_v^2) + \beta^2 c^2 v(\overline{t^2} + t_v^2) \\ & + 2\beta c v[a_{pz}\overline{zt} + a_{px}\overline{xt} + a_{py}\overline{yt} + u_v t_v] = 0 \end{aligned} \tag{49}$$

Table 1
Cost estimates for the 1 Mt AQUA-RICH detector

Item	Quantity	CHF/Unit	MCHF
HPDs, 1 m $\phi(4\pi$ sterad cover)	5310	10 000	53.10
128 ch. pre-amp, 80 MHz FADC chip	21 240	260	5.50
Polymer sheet liner	81 000 m^2	60/m^2	4.90
Kevlar or ss struts for outer geo-dome	100 t	20/kg	2.00
Kevlar or ss struts for inner geo-dome	25 t	20/kg	0.50
HPD containers	5310	600	3.20
Mirror (balloon)	1	2×10^6	2.00
Water pump and purification system	1	4×10^6	4.00
DAQ system	1	1×10^6	1.00
Contingency (10%)	—	—	7.80
Total			84.00

We can then write the general Lagrangian function

$$L \equiv \sum_i h_i^2 + \lambda_1 \overline{s^2}(a_{pz}^2 + a_{px}^2 + a_{py}^2 - 1) + \lambda_2 \bar{s}\bar{h} \quad (50)$$

to be minimized with respect to (u_v,w_v,z_v,t_v), (a_{pz},a_{px},a_{py}) and (λ_1,λ_2). This algorithm uses all the information contained in the blob hit points.

6. Costs and time scale

6.1. The detector

The cost of the 1 Mt AQUA-RICH 4π spherical detector has been estimated in Table 1. The time required to complete this detector will be driven by the time required to prepare the pit. Preparations of the detector components can proceed in parallel. After the pit is available, installation of the detector will probably require an additional 2–3 y.

References

[1] Letter of Intent for Long Baseline RICH, CERN-LAA/96-01, 1/1/96.
[2] T. Ypsilantis et al., Nucl. Instr. and Meth. A 371 (1996) 330.
[3] T. Ypsilantis, J. Seguinot, A. Zichichi, CERN-LAA/96-13, 6/96, Proceedings XXIII SLAC Summer Institute on Particle Physics, SLAC-R-494, 10-21/7/95, pp. 225–260.
[4] M. Honda et al., ICRR-Report-336-95-2.
[5] P. Lipari, Astropar. Phys. 1 (1993) 195.
[6] Y. Fukuda et. al., hep-ex/9807003.
[7] F. Halzen, hep-ex/9809025, 23/9/98.